IEEE Photonics Journal
An IEEE Photonics Society Publication

Open Access

Narrow-Strip Single-Longitudinal-Mode Laser Based on Periodic Anodes Defined by i-Line Lithography

Volume 10, Number 2, April 2018

Feng Gao
Li Qin
Yong-Yi Chen
Peng Jia
Chao Chen
Liwen Cheng
Hong Chen
Lei Liang
Yu-Gang Zeng
Xing Zhang
Yong-Qiang Ning
Li-Jun Wang

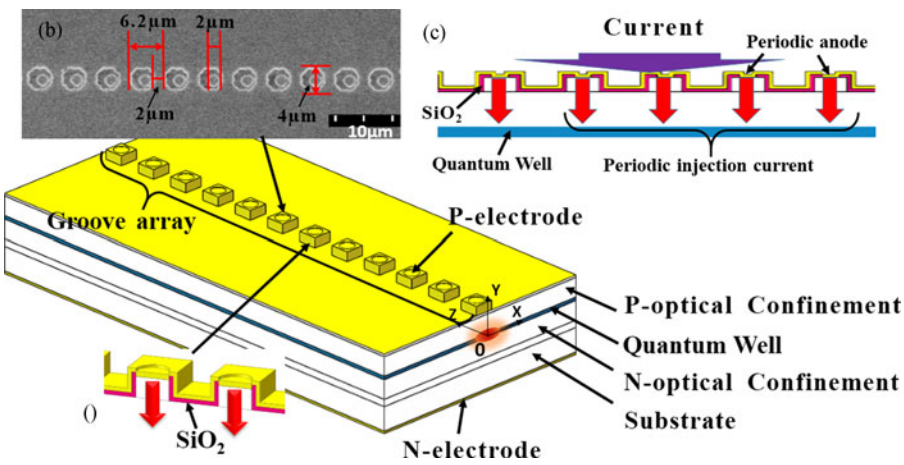

DOI: 10.1109/JPHOT.2018.2818170
1943-0655 © 2018 IEEE

Narrow-Strip Single-Longitudinal-Mode Laser Based on Periodic Anodes Defined by i-Line Lithography

Feng Gao,[1,2] **Li Qin**,[1] **Yong-Yi Chen**,[1] **Peng Jia**,[1] **Chao Chen**,[1] **Liwen Cheng**,[3] **Hong Chen**,[1,2] **Lei Liang**,[1] **Yu-Gang Zeng**,[1] **Xing Zhang**,[1] **Yong-Qiang Ning**,[1] **and Li-Jun Wang**[1]

[1]State Key Laboratory of Luminescence and Application, Changchun Institute of Optics, Fine Mechanics and Physics, Chinese Academy of Sciences, Changchun 130033, China
[2]University of Chinese Academy of Sciences, Beijing 100049, China
[3]College of Physics Science and Technology, Yangzhou University, Yangzhou 225002, China

DOI:10.1109/JPHOT.2018.2818170

Manuscript received February 13, 2018; revised March 7, 2018; accepted March 19, 2018. Date of publication March 22, 2018; date of current version April 10, 2018. This work was supported in part by the National Science and Technology Major Project of China under Grant 2016YFE0126800; in part by the Frontier Science Key Program of President of the Chinese Academy of Sciences under Grant QYZDY-SSW-JSC006; in part by the National Natural Science Foundation of China under Grants 61234004, 51672264, 61674148, 11604328, 11404327, 61505206, and 61235004; and in part by the Natural Science Foundation of Jilin Province (Jilin Province Natural Science Foundation) under Grants 20160520017JH, 20170623024TC, 20180201014GX, 20150203007GX, 20150204042GX, and 20160414016GH. Corresponding authors: Y.-Y. Chen, P. Jia, and C. Chen (e-mail: chenyy@ciomp.ac.cn; jiapeng@ciomp.ac.cn; chenc@ciomp.ac.cn).

Abstract: A low-cost regrowth-free narrow-strip single-longitudinal-mode diode laser, based on periodic anodes defined only by i-line lithography is proposed. With the periodic anodes separated by surface insulated grooves acting as a 44th-order gain grating, a high gain contrast is achieved without introducing effective index coupling. The CW output power of the device without facet coatings is up to 100.9 mW/facet at 980.63 nm in single-longitudinal-mode operation with a single facet having a power conversion efficiency of up to 18.6% and a slope efficiency of 0.53 W/A. The highest side-mode suppression ratio is 45 dB with a linewidth below 889 MHz, at 350 mA. The beam parameter product, M^2, in the slow axis is 1.85, achieving a near diffraction-limited beam quality. A novel method for easy surface gratings fabrication is first presented, wherein, 4-μm-width periodic surface grooves, acting as waveguide ridges, are defined once by i-line lithography only without regrowth, nanoscale gratings fabrication, or facet coating. Owing to the low-cost fabrication methods and good performances, our single-longitudinal-mode devices can be used for widespread practical applications.

Index Terms: Semiconductor lasers, single longitudinal mode, narrow linewidth.

1. Introduction

Single-longitudinal-mode diode lasers are extensively used as light sources in high-efficiency pumping sources for alkali atom-based clocks or fiber lasers [1], for accurate gas sensing and detection in spectroscopy [2], coherent light detection and ranging (LIDAR) used in robotic vision, for non-contact surface profiling, high-speed servo control loops, fault detection in optical fibers [3], [4],

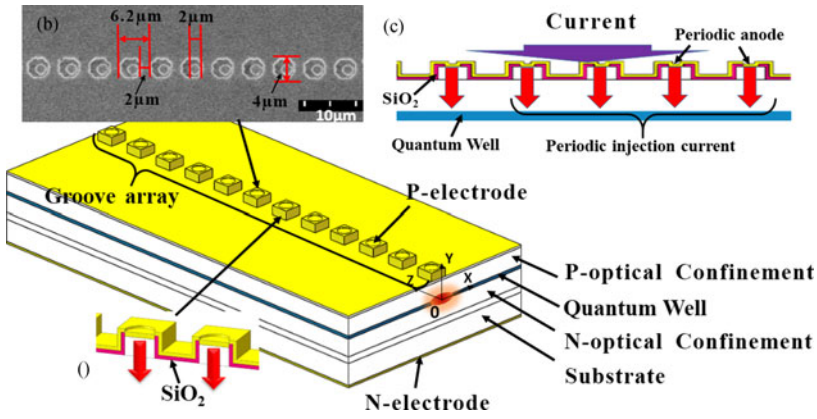

Fig. 1. Device schematic (a) Cross-section of periodic anodes, (b) Scanning electron microscope image of the top of the p-electrodes, and (c) Periodic current injection operation schematic.

integrated optics [5], [6]. Mode selective structures like gratings are widely used to filter high-order longitudinal modes to gain single-longitudinal-mode operation. Index-coupled Bragg gratings with feedback effect provided by a periodic change of refractive index could be one solution. However, there is an intrinsic problem of lasing two degenerated modes [7]. Although high-quality asymmetrical facet coatings [8] may offer a solution, devices continue to suffer from random facet phases [9], which are hard to control, influencing the single-longitudinal-mode yield. The introduction of a phase shift in gratings [10] or the use of the reconstruction-equivalent-chirp (REC) technique based on the sampled Bragg grating [11], [12], also offer a single-longitudinal-mode operation; however, they both require complex fabrication such as the second epitaxy or delicate nanoscale grating fabrication and both the facets in the devices must be anti-reflection coated. Output lasing occurs at both the facets, leading to a waste of half the energy from the generated laser.

Gain-coupled Bragg grating is another choice for achieving a single longitudinal mode [7], with the feedback effect being provided by a periodic change of the gain (or loss). Gain-coupled gratings can effectively remove mode degeneracy [13], realizing a high single-longitudinal-mode yield [14], facet immunity [15], ultra-low chirping [16] a high gain margin [17], [18], which are all the key characteristics for photonic devices in practical applications. However, traditional processing also requires complex technology including high-cost, time-consuming nanoscale grating fabrication and epitaxial regrowth, further increasing the cost, without enhancing the processing of the index-coupled gratings; this has prevented the extensive use of diode lasers with gain-coupled gratings in practical manufacture till date.

To solve these problems, we propose a novel regrowth-free low-cost narrow-strip diode laser with periodic anodes to realize single-longitudinal-mode operation. The enhancing fabrication processing is that 4-μm-width periodic surface grooves, acting as waveguide ridges, were patterned once, using only i-line lithography without complex fabrication steps or high-quality facet coating technology. Moreover, with such a simple and robust technique, our devices still obtain a good performance, benefitting from high continuous-wave (CW) power ($>$100.9 mW/facet, at the same level of reported high power single-longitudinal-mode lasers [19]), high side mode suppression ratio (SMSR) ($>$43 dB, larger than diode lasers with nanoscale gratings [20], [21]), narrow linewidth ($<$889 MHz, much better than single-mode laser with surface high-order gratings [22]). Our devices' fabrication technology can effectively reduce the fabrication costs of single-longitudinal-mode lasers, having a potential for widespread practical applications.

2. Structure and Fabrication

The schematic diagram of our devices is shown in Fig. 1. Periodic grooves are insulated by silica and periodic anodes were defined on the unetched periodic areas, as show in Fig. 1(a). The entire ridge waveguide is etched into discontinued ridge islands separated by the groove array.

TABLE 1
Epitaxial Structures for Narrow-Strip Single-Longitudinal-Mode Laser Based on Periodic Anodes Defined by i-Line Lithography

Layer	Composition	Thickness(nm)
1 Cap	p+:GaAs	120
2 P-cladding	p:AlGaAs	500
3 P-optical confinement	p: AlGaAs	1200
4 QWs	GaAs&InGaAs	32
5 N-optical confinement	p: AlGaAs	3000
6 N-cladding	p:AlGaAs	600
7 Substrate	n+:GaAs	~350000

The discontinued ridge islands are patterned simultaneously when the groove array and the mesa are etched together. The period is chosen as 6.2 μm to allow only 44th order Bragg wavelength in the total gain spectrum, meanwhile maintain process compatible with i-line lithography, with groove length of 2 μm as shown in Fig. 1(b). Comparing with the single-longitudinal-mode with nanoscale grating period [7]–[15], the large period in our device can be easily fabricated by i-line lithography, suitable for the mass production. Moreover, in this work, a novel method for surface gratings fabrication is first presented, wherein, 4-μm-width periodic surface grooves, acting as waveguide ridges, are patterned once by i-line lithography only and etched to the same depth (520 nm), further simplifying the fabrication processing. Injection current transmits through these periodic anodes, as shown in Fig. 1(c), leading to periodic carrier density distribution in quantum wells. Since grooves could effectively reduce the drift of carriers, the contrast of carrier density could be formed in quantum wells. Due to the linear relationship between the carrier density and the optical gain [23], it results in periodic gain contrasts in the quantum wells, forming gain-coupled mechanism.

The fabrication processing of our device is simple and requires only five key steps: 1) Epitaxial structure growth, 2) groove patterning, 3) periodic current injection window patterning, 4) metallization, and 5) cleavage and test. The epitaxy as shown in Table 1 was grown by Metal Organic Chemical Vapor Deposition (MOCVD), including two InGaAs quantum wells emitting around 970 nm, which were embedded in a large optical cavity, consisting of 1.2 μm and 3 μm p- and n-doped $Al_{0.1}Ga_{0.9}As$ optical confinement with 200 nm GaAs p-cap layer. The 4-μm-width periodic surface grooves, acting as waveguide ridges, were patterned once by i-line lithography only and etched to 520 nm by an inductively coupled plasma (ICP) machine. Then, a silica layer with suitable thickness was deposited on top of the epitaxy by plasma enhanced chemical vapor deposition (PECVD) and the periodic anode [the length of 2 μm and the width of 2 μm, as shown in Fig. 1(b)] was also patterned by i-line lithography. After metallization, a surface periodic metal p-contact was formed. The thickness of the chip was then reduced and polished for N-contact metallization. Finally, the chips were cleaved to 2 mm-length devices, without facet coating. The devices were mounted p-side down on simple Cu C-mount heat sinks without precise temperature control like Thermo Electric Cooler (TEC), and placed on a water-cooling unit at 20°C for testing, under a continuous-wave (CW) operation.

3. Theory and Simulation

To better understand the operating mechanism of our single-longitudinal-mode lasers with easy fabrication, the coupling coefficient κ should be calculated and discussed because index-coupled

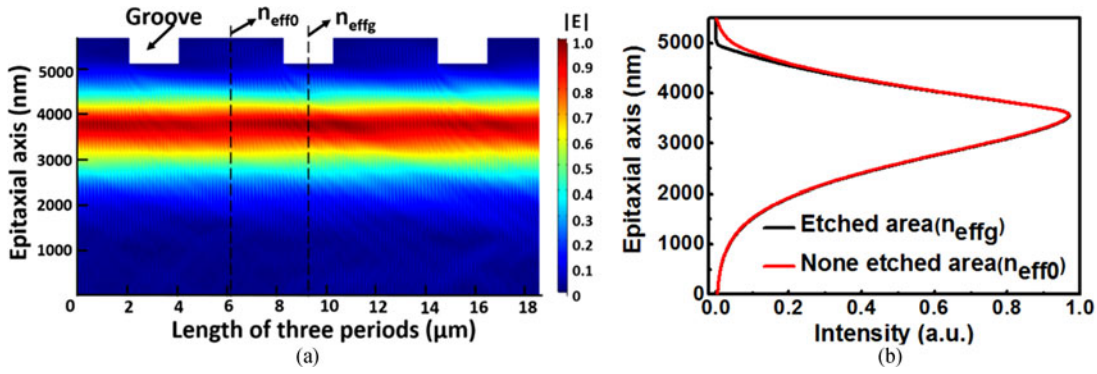

Fig. 2. (a) Calculated mode propagation characteristics along the cavity for three periods (b) Calculated mode distribution along the epitaxial axis for etched area and none etched area.

effect could be also introduced by surface grooves. Since the real part of κ represents feedback strength of index-coupled mechanism while the imaginary represents gain-coupled mechanism. The change of refractive index and nonuniform carrier density distribution introduced by surface insulated grooves was calculated by the commercial software Comsol Multiphysics and PICS3D, respectively. κ represents the coupling coefficient [24], [25]:

$$\kappa = \frac{{k_0}^2 \bar{n}_{eff}}{\beta_0} \frac{\int_{-\infty}^{+\infty} \Delta n_p(z)\, U^2(x,y)\, dz}{\int_{-\infty}^{+\infty} U^2(x,y)\, dz} \tag{1}$$

where, $k_0 = \frac{2\pi}{\lambda_0}$ is the vacuum wave number for the vacuum wavelength λ_0. $\bar{n}_{eff}$ is the average mode effective index of the Bragg grating structure. β_0 is propagation constant. $U(x, y)$ is the mode pattern. $\Delta\tilde{n}_p(z)$ is the Fourier factor of the p_{th} Fourier expansion for the mode effective index difference $\Delta\tilde{n}(z)$:

$$\Delta\tilde{n}(z) = \sum_{l=-\infty}^{\infty} \Delta\tilde{n}_p e^{j2\beta_B z}. \tag{2}$$

where, β_B represents the Bragg wave vector.

Noting that, when we consider the gain/loss and the refractive index change in the waveguide,

$$\Delta\tilde{n}(z) = \Delta n(z) + i\frac{\Delta g(z)}{2k_0}. \tag{3}$$

where, $\delta g(z)$ represents the gain/loss change in the waveguide, and $\delta n(z)$ is the refractive index change.

Consider a single period, and choose the center of the groove as original spot as shown in the inset in Fig. 1(a). Considering carrier vertical injection and side drift, we assume a cosine shape for the carrier density in the waveguide. As a liner relationship between model gain and carrier density [23], we have a cosine-shaped gain. Hence the rectangular form of index grating and cosine shape of gain are written as below:

$$\Delta n(z) = \Delta n = \begin{cases} n_{eff0} - n_{effg} & \left(-\frac{L_g}{2} \le z \le \frac{L_g}{2}\right) \\ 0 & \left(-\frac{\Lambda}{2} \le z \le -\frac{L_g}{2}, \frac{L_g}{2} \le z \le \frac{\Lambda}{2}\right) \end{cases} \tag{4}$$

$$\Delta g(z) = \Delta g cos\left(\frac{2l\pi}{\Lambda} z + \pi\right) \tag{5}$$

where, n_{eff0} is the mode effective index of the none etched area, and n_{effg} is the mode effective index of the etched area with 520 nm depth as shown in Fig. 2(a). L_g represents the grating's groove length. Δn is the refractive index change in the waveguide. Λ is the period for the l order grating ($\Lambda = l\lambda/2\bar{n}_{eff}$).

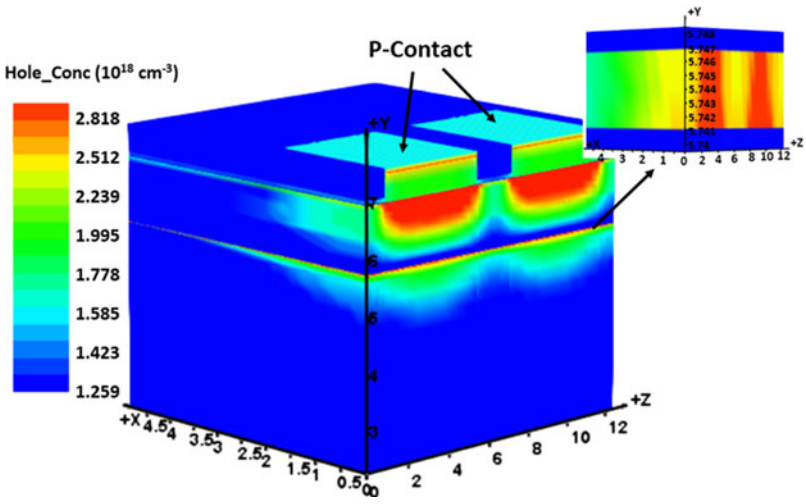

Fig. 3. Three-dimensional carrier density distribution for two periods (x: Lateral axis. y: Epitaxial axis. z: Device cavity axis.). The inset shows the 3D carrier density distribution in the quantum well.

As the Fourier transform based on (2),

$$\Delta\tilde{n}_p(z) = \frac{1}{\Lambda}\int_{-\frac{\Lambda}{2}}^{\frac{\Lambda}{2}} \Delta\tilde{n}(z)\, e^{j2\beta_B z} dz, \tag{6}$$

We have,

$$\Delta\tilde{n}_{+1}(z) = \Delta n \frac{\sin\left(\frac{l\pi}{\Lambda} L_g\right)}{l\pi} + i\frac{\Delta g}{4k_0} \tag{7}$$

Considering $\bar{n}_{eff} \approx n_{eff_0} \approx n_{eff_g}$, the theoretical calculation for κ is

$$\kappa = k_0 \Gamma' \Delta n \frac{\sin\left(\frac{l\pi}{\Lambda} L_g\right)}{l\pi} + i\frac{\Delta g \Gamma}{4} \tag{8}$$

where, Γ' is the optical confinement in the gratings. Γ is the optical confinement factor in the quantum wells.

The cross-sectional mode propagation characteristics along the cavity for three periods is calculated by the commercial software COMSOL Multiphysics as shown in the Fig. 2(a) with the original point at the top of substrate along the epitaxial axis. And mode effective index is 3.448 in the none etched area while 3.447 in the etched area with 520 nm depth. The surface groove also leads to different mode distribution along the epitaxial axis, as shown in Fig. 2(b). A higher order period (6.2 μm, 44th order grating) and a smaller difference in the effective index, Δn (0.001, varying from 3.448/none etched region to 3.447/etched region with 520 nm depth with $\Gamma' = 1.1578 \times 10^{-4}$, numerically calculated by the commercial software COMSOL Multiphysics) lead to the calculated real part of κ only 0.0031 m^{-1}. κL is always considered as the total index-coupling strength and for a cavity with length $L = 2\ mm$, the calculated κL is only 6.2×10^{-6}. Since κL is greater than 1 for index-coupled Bragg gratings [26], [27] and even 0.3 for high-order index Bragg gratings lasers working in the multiple longitudinal mode [28]. The index-coupled effect in our devices is far weaker and could not provide effective index-coupling feedback to form single-longitudinal-mode operation.

To analyze the imaginary part of κ, carrier density distribution is calculated by the commercial software PICS3D. Fig. 3 shows the calculated carrier density distribution for two periods, indicating the formation of carrier density contrast in quantum wells. As gain is linearly proportional to the carrier density [23], periodic gain contrast in quantum wells would be formed, leading to gain-coupled effect. Fig. 4 depicts the carrier density distribution in the quantum well with a peak-to-valley contrast above 2.99×18 cm^{-3}. And the shape of the carrier density distribution fits a cosine curve due to

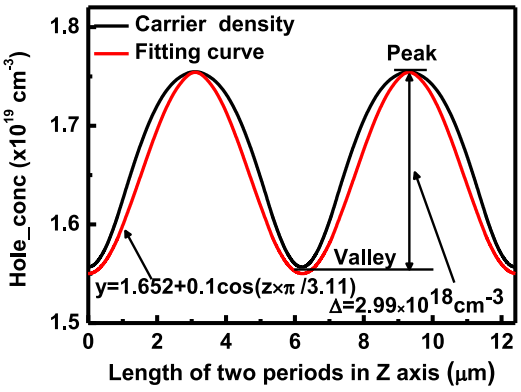

Fig. 4. One-dimensional carrier density distribution in one quantum well for two periods.

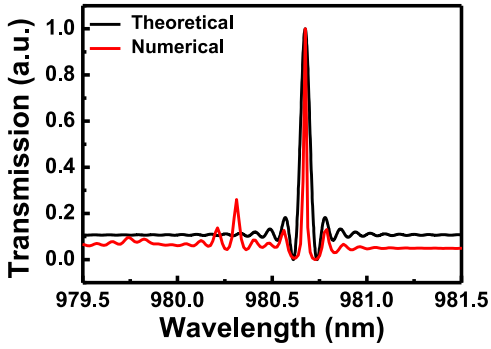

Fig. 5. Calculated transmission spectrum for the theoretical and numerical analyses.

the drift of carrier. For the gain material of InGaAs, gain contrast δg is 584 cm^{-1} according to the linear relationship between carrier density and material gain provided by the commercial software PICS3D. With $\Gamma = 0.01185$ calculated by the commercial software COMSOL Multiphysics, the imaginary part of κ is calculated to be 1.73 cm^{-1}. Compared with the reported stable single-mode gain-coupled gratings with the imaginary part of κ 1.25 cm^{-1} and the cavity length 400 μm [29], our devices with 2-mm cavity length could provide enough gain-coupled feedback strength to achieve single-longitudinal-mode operation. And the imaginary part of κ could be further enhanced by reducing the thickness of p-optical confinement or increasing the groove length.

As gain-coupled gratings could remove mode degeneracy, there is only one peak in the transmission spectrum of gain-coupled gratings without stop band of index-coupled. Hence, the transmission spectrum for our devices was calculated based on the coupled-mode theory mentioned in the reference [24], which can be expressed by

$$T = \left| \frac{1 - r_a r_b}{e^{-iqL} - r_a r_b e^{iqL}} \right|^2 \tag{9}$$

An analytical solution of transmission spectrum can be drawn from (9), using the transmission matrix [30] method to analyze the S parameters [31]. The data of carrier density distribution and gain-spectrum calculated by software PICS3D were extracted and transferred to the commercial software COMSOL Multiphysics and the transmission matrix elements were numerically calculated. The theoretical and numerical transmission spectrum as a function of the wavelength was then calculated by coding from the S parameters, as shown in Fig. 5. There is only one lasing mode in both theoretical and numerical analyses, assuring our device operates as gain-coupled mechanism.

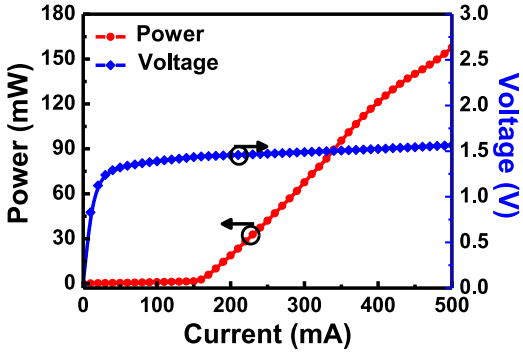

Fig. 6. Measured power-voltage-current characteristics in CW mode at 20°C.

4. Results and Discussion

The measured power-voltage-current characteristics for our low-cost single-longitudinal-mode device without facet coating in CW operation are shown in Fig. 6. The threshold current was about 152 mA. The threshold current is still a relatively high compared with that of some previous reports. This may result from the surface grooves. Periodic grooves actually coupled a small part of waveguide power acting as index-coupled gratings. On the other hand, the total optical loss (like scattering loss brought by etched groove sidewalls, which are not smooth) suffer from 0.05% power loss for one period calculated by the commercial software COMSOL Multiphysics. Since this is our initial try experimentally for this structure, we can achieve better characteristics with improved fabrication techniques. And the slope efficiency was up to 0.53 W/A, five times larger than 0.11 W/A of the previously reported gain-coupled lasers with a titanium surface Bragg gratings, benefitting from removing the loss introduced by metallic surface Bragg gratings [32]. The power conversion efficiency of a single facet was up to 18.6%. This high-power conversion efficiency was owing to two factors: First, the weak index coupling effect reduced most of the scattering loss, compared to the other surface high-order index-coupled gratings [28] and the high order grooves in a finite cavity length of 2 mm reduce the number of periods, further reducing the index coupling effect. Secondly, a large period with narrow grooves resulted in a better ohmic p-contact with a low resistance. Because the periodic current originated from the highly p-doped regions without the interruption of the highly p-doped top layer, avoiding the forming of a complex p-contact as in ordinary surface gratings, as mentioned in reference [33]. The maximum output power of per facet, in a single-longitudinal-mode operation at 360 mA was 100.9 mW. This is a high power, attaining the same energy level of the single-longitudinal-mode index-coupled lasers [19], which could be further improved by anti-reflection and high-reflection (AR/HR) facet coating technology, owing to facet immunity of gain coupling mechanism [15].

Our low-cost narrow-strip devices defined only by i-line lithography without facet coating realized single-longitudinal-mode operation by periodic injection current. Without structure regrowth or nanoscale gratings, it was defined by i-line lithography, reducing time consumption and cost. Fig. 6 shows the CW spectrum characteristics with different injection currents measured by an optical spectrum analyzer (YOKOGAWA AQ6370C). The highest SMSR was 45 dB at 350 nm, as depicted in Fig. 7(b), larger than the lasers with nanoscale gratings [20], [21]. While the Fabry-Perot (FP) lasers with the uniform current injection, fabricated on the same chip for comparison, were operating at multi-longitudinal modes, as shown in the inset of Fig. 7(b). It's because the periodic injection current could introduce gain-coupled mechanism, filtering out additional modes and guaranteeing single-longitudinal-mode operation. The 3dB spectrum linewidth measured by coupling collimating laser to Fabry-Perot Interferometer (Thorlabs, SA200-8B) with the oscilloscope was only 889 MHz (2.84 pm), which was much better than the reported lasers with surface high-order index-coupled gratings (10 pm) [22]. At 360 mA, the actual lasing wavelength of the device was 980.63 nm, close to the Bragg wavelength of 980.68 nm as shown in Fig. 4. A minor difference is probably

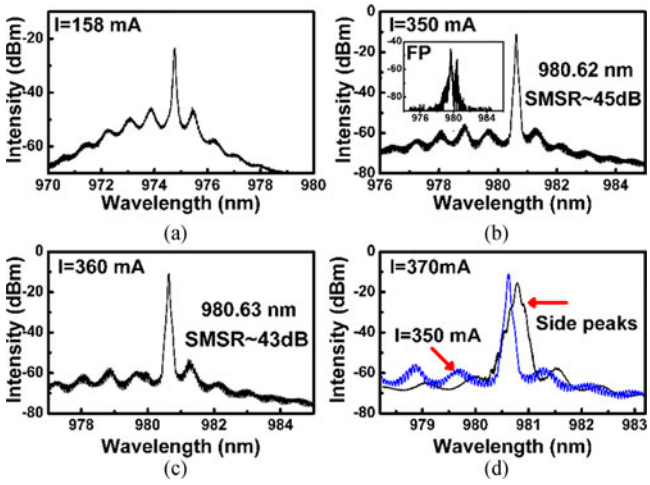

Fig. 7. CW spectrum characteristics (a) 158 mA (b) 350 mA (inset: Fabry-Perot (FP) laser at 350 mA), (c) 360 mA, and (d) 370 mA.

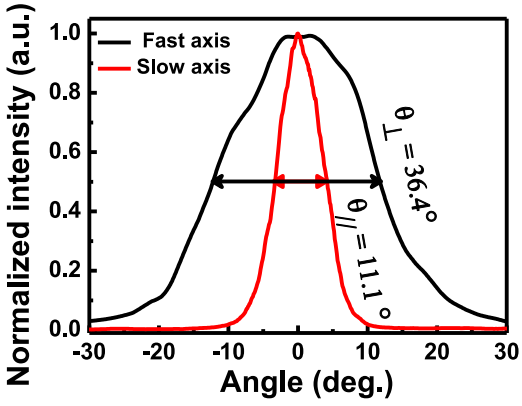

Fig. 8. Measured far-field pattern in the CW mode at 360 mA.

caused by the theoretical refractive index, which is different from the actual material in the epitaxial wafer, owing to current injection or heat accumulation. There is only one lasing mode in the theoretical and numerical analyses, and in the experimental test, establishing that our device operates as a gain-coupled mechanism. With the current increasing over 360 mA, side peaks on the main lasing peak begin to emerge, as shown in Fig. 7(d). One reason for the broadening linewidth is that high injection current may saturate the laser junction, which would weaken the gain-coupled effect. The other is caused by the Fabry-Perot (FP) modes generated from the uncoated facet reflection and can be removed by AR-HR facet coating to enlarge the single-longitudinal mode operation range with higher output power.

Measured far-field pattern in CW mode at 360 mA is shown in Fig. 8. The beam divergence at full width at half maximums (FWHM) was 11.1° for the slow axis and 36.2° for the fast axis. Based on the 2σ value of the Gaussian, fitting the near field diameter (11.8 μm) and the far field angle (11.1°), the value of the beam propagation factor, M^2, in the slow axis was only 1.85. Owing to the fact that the 4-μm-width ridge provides index-guiding and filters out high-order lateral modes, our devices have achieved a nearly diffraction-limited beam quality along the lateral direction, especially suitable for fiber coupling as pumping sources for fiber laser or solid-state laser systems.

5. Conclusion

A narrow-strip, regrowth-free single-longitudinal-mode laser based on periodic anodes defined by i-line lithography was demonstrated without regrowth, precise nanoscale grating fabrication or facet coatings. With periodic anodes separated by surface insulated grooves acting as a 44th-order gain grating, a high gain contrast is achieved without introducing effective index coupling. The CW output power of the devices without facet coatings is up to 100.9 mW/facet at the same level of reported high power single-longitudinal-mode lasers [19]. And the slope efficiency was up to 0.53 W/A, five times larger than 0.11 W/A of the previously reported lasers with a titanium surface gain-coupled Bragg gratings [30]. The power conversion efficiency of a single facet was up to 18.6%. High side mode suppression ratio (SMSR) is larger than diode lasers with nanoscale gratings [20], [21] and narrow linewidth ($<$889 MHz) is much better than single-mode laser with surface high-order gratings [22]. The beam parameter product, M^2, in the slow axis is 1.85, achieving a near diffraction-limited beam quality, laterally. A novel method for easy surface gratings fabrication is presented, wherein, 4-μm-width periodic surface grooves, acting as waveguide ridges, are defined once by i-line lithography only. This novel method for low-cost narrow-strip single-longitudinal-mode diode lasers defined only by i-line lithography without facet coating could be used for widespread practical application like pumping source, especially in integrated optics owing to easy fabrication to achieve single-longitudinal-mode operation without facet coating, regrowth or complex fabrication.

References

[1] R. Paschotta, J. Nilsson, A. C. Tropper, and D. C. Hanna, "Ytterbium-doped fiber amplifiers," *IEEE J. Quantum Electron.*, vol. 33, no. 7, pp. 1049–1056, Jul. 1997.

[2] H. Jeon, J. M. Verdiell, M. Ziari, and A. Mathur, "High-power low-divergence semiconductor lasers for GaAs-based 980-nm and InP-based 1550-nm applications," *IEEE J. Sel. Topics Quantum Electron.*, vol. 3, no. 6, pp. 1344–1350, Dec. 1998.

[3] E. C. Burrows and K. Y. Liou, "High resolution laser LIDAR utilising two-section distributed feedback semiconductor laser as a coherent source," *Electron. Lett.*, vol. 26, no. 9, pp. 577–579, 1990.

[4] B. W. Tilma *et al.*, "Recent advances in ultrafast semiconductor disk lasers," *Light Sci. Appl.*, vol. 4, no. 7, 2015, Art. no. e310.

[5] Z. Zhou, B. Yin, and J. Michel, "On-chip light sources for silicon photonics," *Light Sci. Appl.*, vol. 4, no. 11, 2015, Art. no. e358.

[6] C. García-Meca *et al.*, "On-chip wireless silicon photonics: From reconfigurable interconnects to lab-on-chip devices," *Light Sci. Appl.*, vol. 6, no. 9, 2017, Art. no. e17053.

[7] H. Kogelnik and C. V. Shank, "Coupled-wave theory of distributed feedback lasers," *J. Appl. Phys.*, vol. 43, no. 5, pp. 2327–2335, 1972.

[8] S. R. Chinn, "Effects of mirror reflectivity in a distributed-feedback laser," *IEEE J. Quantum Electron.* vol. 9, no. 6, pp. 574–580, Jun. 1973.

[9] H. Haus and C. V. Shank, "Antisymmetric taper of distributed feedback lasers," *IEEE J. Quantum Electron.*, vol. 12, no. 9, pp. 532–539, Sep. 1976.

[10] H. Soda, Y. Kotaki, H. Sudo, and H. Ishikawa, "Stability in single longitudinal mode operation in GaInAsP/InP phase-adjusted DFB lasers," *IEEE J. Quantum Electron.*, vol. 23, no. 6, pp. 804–814, Jun. 1987.

[11] J. Li *et al.*, "Experimental demonstration of distributed feedback semiconductor lasers based on reconstruction-equivalent-chirp technology," *Opt. Exp.*, vol. 17, no. 7, pp. 5240–5245, 2009.

[12] Y. Shi, S. Li, R. Guo, R. Liu, Y. Zhou, and X. Chen, "A novel concavely apodized DFB semiconductor laser using common holographic exposure," *Opt. Exp.*, vol. 21, no. 13, pp. 16022–16028, 2013.

[13] Y. Nakano, Y. Luo, and K. Tada, "Facet reflection independent, single longitudinal mode oscillation in a GaAlAs/GaAs distributed feedback laser equipped with a gain coupling mechanism," *Appl. Phys. Lett.*, vol. 55, no. 16, pp. 1606–1608, 1989.

[14] N. Susa, "Fluctuations of the laser characteristics and the effect of the index-coupling component in the gain-coupled DFB laser," *IEEE J. Quantum Electron.*, vol. 33, no. 12, pp. 2255–2265, Dec. 1997.

[15] L. M. Zhang and J. E. Carroll, "Enhanced AM and FM modulation response of complex coupled DFB lasers," *IEEE Photon.Technol. Lett.*, vol. 5, no. 5, pp. 506–508, May 1993.

[16] Y. Luo, Y. Nakano, K. Tada, and T. Inoue, "Fabrication and characteristics of gain-coupled distributed feedback semiconductor lasers with a corrugated active layer," *IEEE J. Quantum Electron.*, vol. 27, no. 6, pp. 1724–1731, Jun. 1991.

[17] Y. Luo, Y. Nakano, K. Tada, T. Inoue, H. Hosomatsu, and H. Iwaoka, "Purely gain-coupled distributed feedback semiconducutor lasers," *Appl. Phys. Lett.*, vol. 56, no. 17, pp. 1620–1622, Apr. 1990.

[18] A. J. Lowery and D. Novak, "Performance comparison of gain-coupled and index-coupled DFB semiconductor lasers," *IEEE J. Quantum Electron.*, vol. 30, no. 9, pp. 2051–2063, Sep. 1994.

[19] S. Spiebberger, M. Schiemangk, A. Wicht, H. Wenzel, O. Brox, and G. Erbert, "Narrow linewidth DFB lasers emitting near a wavelength of 1064 nm," *J. Lightw. Technol.*, vol. 28, no. 17, pp. 2611–2616, Sep. 2010.
[20] Y. Luo, Y. Nakano, K. Tada, T. Inoue, H. Hosomatsu, and H. Iwaoka, "Purely gain-coupled distributed feedback semiconductor lasers," *Appl. Phys. Lett.*, vol. 56, no. 17, pp. 1620–1622, Apr. 1990.
[21] L. Liu, H. Qu, Y. Wang, Y. Liu, Y. Zhang, and W. Zheng, "High-brightness single-mode double-tapered laser diodes with laterally coupled high-order surface grating," *Opt. Lett.*, vol. 39, no. 11, pp. 3231–3234, 2014.
[22] T. N. Vu, A. Klehr, B. Sumpf, H. Wenzel, G. Erbert, and G. Tränkle, "Tunable 975 nm nanosecond diode-laser-based master-oscillator power-amplifier system with 16.3 W peak power and narrow spectral linewidth below 10 pm," *Opt. Lett.*, vol. 39, no. 17, pp. 5138–5141, 2014.
[23] B. W. Hakki, "Carrier and gain spatial profiles in GaAs stripe geometry lasers," *J. Appl. Phys.*, vol. 44, no. 11, pp. 5021–5028, 1973.
[24] S. L. Chuang, *Physics of Photonic Devices*. New York, NY, USA: Wiley, 2009.
[25] B. Jonsson, A. J. Lowery, H. Olesen, and B. Tromborg, "Instabilities and nonlinear L-I characteristics in complex-coupled DFB lasers with antiphase gain and index gratings," *IEEE J. Quantum Electron.*, vol. 32, no. 5, pp. 839–850, May 1996.
[26] M. Kanskar, Y. He, J. Cai, and C. Galstad, "53% wallplug efficiency 975nm distributed feedback broad area laser," *Electron. Lett.*, vol. 42, no. 25, pp. 1455–1457, 2006.
[27] Y. He, H. An, J. Cai, and C. Galstad, "808 nm broad area DFB laser for solid-state laser pumping application," *Electron. Lett.*, vol. 45, no. 3, pp. 163–164, 2009.
[28] J. Decker, P. Crump, J. Fricke, A. Maassdorf, G. Erbert, and G. Trankle, "Narrow stripe broad area lasers with high order distributed feedback surface gratings," *IEEE Photon.Technol. Lett.*, vol. 26, no. 8, pp. 829–832, Apr. 2014.
[29] R. G. Baets, K. David, and G. Morthier, "On the distinctive features of gain coupled DFB lasers and DFB lasers with second-order grating," *IEEE J. Quantum Electron.*, vol. 29, no. 6, pp. 1792–1798, Jun. 1993.
[30] H. Zhu, Y. Xia, and J. J. He, "Pattern dependence in high-speed Q-modulated distributed feedback laser," *Opt. Exp.*, vol. 23, no. 9, pp. 11887–11897, 2015.
[31] P. Jia *et al.*, "Broad-stripe single longitudinal mode laser based on metal slots," *Opt.Commun.*, vol. 365, pp. 215–219, 2016.
[32] T. W. Johannes, A. Rast, W. Harth, and J. Rieger, "Gain-coupled DFB lasers with a titanium surface Bragg grating," *Electron. Lett.*, vol. 31, no. 5, pp. 370–371, 2002.
[33] H. Wenzel, J. Fricke, J. Decker, and P. Crump, "High-power distributed feedback lasers with surface gratings: Theory and experiment," *IEEE J. Sel. Topics Quantum Electron.*, vol. 21, no. 6, Nov./Dec. 2015, Art. no. 1502707.